ELSEVIER

Journal of Nuclear Materials 297 (2001) 220–229

journal of nuclear materials

www.elsevier.com/locate/jnucmat

Diffusion reaction between Zr–2.5 wt% Nb alloy and martensitic grade 403 stainless steel

K. Bhanumurthy *, R.V. Patil, D. Srivatsava, P.S. Gawde, G.B. Kale

Materials Science Division, Bhabha Atomic Research Centre, Trombay, Mumbai 400 085, India

Received 2 July 1999; accepted 2 April 2001

Abstract

Diffusion reaction between Zr–2.5 wt% Nb alloy and 403 stainless steel has been investigated by employing miniature type diffusion couples in the temperature range between 750°C and 940°C for 1–240 h. An electron probe microanalyser (EPMA) has been used to establish the concentration penetration profiles across the diffusion zone and a transmission electron microscope (TEM) has been used to identify various phases formed close to the interface. The microstructure of the bonded region on the 403 steel side is essentially a martensitic structure and remains nearly unchanged during annealing. However, the microstructure of the Zr–2.5 wt% Nb alloy changes substantially, leading to the formation of coarser α phase. The diffusion reaction is extremely sluggish. Localised melting occurs in the specimens annealed at and above 940°C. This is essentially due to the eutectic reaction between zirconium and iron. The experiments confirm that diffusion bonding of 403 steel to Zr–2.5 wt% Nb could be carried out at a pressure of 10 MPa at 900°C for 1 h. The formation of various phases in this multi-phase and multi-component system along with change in their composition with annealing temperature and the nature of reaction products is discussed.

1. Introduction

The structural materials inside the core of the reactor in the pressurised heavy water reactors (PHWR) are basically zirconium base alloys like Zircaloy-2 (Zr-2), Zr–2.5 wt% Nb (Zr–2.5Nb) etc. due to their superior mechanical and corrosion properties and also due to low absorption cross-section for thermal neutrons. Zirconium being expensive, its use is restricted only to in-core components of the reactor. Outside the reactor core, carbon steels which are most cost effective are used. This requires the joining of the two materials. Conventional fusion welding between Zr alloys and steels is unacceptable due to the formation of brittle intermetallic compounds like $ZrFe_2$ and $ZrFe_3$ in the fusion zone [1]. Alternatively, a variety of mechanically rolled joints are used for a range of geometries for PHWR core components. The two geometries, which require these joints, include the pressure tube to end fitting and calendria tube to tube sheet. These rolled joints are highly stressed particularly in the grooves, where maximum plastic deformation takes place. These grooves become the active centers for hydrogen pickup and may result in cracking [2].

In view of these difficulties several researchers have tried joining these materials by solid state bonding. Solid state bonding involves joining these materials at 50–70% of the melting point of the most fusible material, at a predetermined time (t) and pressure (p). Shaaban et al. [3] have carried out direct diffusion bonding between Zircaloy-4 and austenitic steel (AISI 304) and reported the formation of brittle intermetallic compounds in the diffusion zone. Various workers have used different diffusion barriers to minimise or prevent the formation of brittle compounds in order to facilitate good solid state bonding. Kale et al. have tried Ti, Fe [4] and recently Bhanumurthy et al. have used Nb, Cu, Ni multi-layers for bonding Zircaloy-2 to austenitic stainless steel [5–7]. Only limited work has been carried out on diffusion bonding of Zr–2.5Nb with steels. Cooper [8] has devel-

* Corresponding author.

0022-3115/01/$ - see front matter
PII: S0022-3115(01)00600-6

oped direct bonding of Zr–2.5Nb with ASTM A 106B carbon steel. However, detailed microstructural characterization of the interface was not attempted. Wayman et al. [9] have carried out bonding of Zr–2.5Nb to carbon steel (ASTM A106B) with Pt interlayer in the temperature range 1000–1250°C over a pressure range 9–35 MPa. Though these studies suggested a satisfactory bond, they confirmed the formation of Pt_3Zr and $Pt_{11}Zr_9$, intermetallic compounds in the reaction zone. In view of the limited studies, a detailed investigation on the diffusion reaction between Zr–2.5Nb and 403 steel has been attempted. The main objectives of the investigations are:

- to join miniature samples of Zr–2.5Nb to 403 steel by diffusion bonding without using any intermediate layers;
- to characterise the bonded interface using analytical techniques like optical metallography, scanning electron microscopy (SEM), transmission electron microscopy (TEM) and electron probe microanalysis (EPMA).

2. Experimental work

The present studies involved several steps including, preparation of sandwich type diffusion couples, diffusion annealing, establishment of true concentration profiles by EPMA and characterisation of the reaction products by TEM. The details are mentioned below.

2.1. Preparation of diffusion couple

The Zr–2.5Nb samples obtained from Nuclear Fuel Complex, Hyderabad (NFC) and commercial grade 403 steel in the form of sheets were used in these studies. The chemical composition of these samples is listed in Table 1. The rectangular samples of approximately $10 \times 5 \times 3$ mm^3 dimensions were cut from these sheets. These specimens were metallographically polished to 1 μm diamond finish, followed by light etching to remove the cold worked layer. 'Sandwich' type diffusion couples were made from the metallographically polished specimen by pressure bonding technique. A special die made up of Invar was designed for keeping the polished surfaces in contact with each other. Mica sheet spacers were used to prevent direct contact between the die and the couple in order to avoid any undesirable reaction with the die. The specimens were bonded at 700–900°C for 1 h under a pressure of 5–15 MPa. Generally the specimens joined below 900°C and at a pressure below 10 MPa resulted in poor quality of bonding across the interface. An optimum pressure of 10 MPa was essential for joining these specimens. However, bonding of the specimens at 900°C at a pressure of 15 MPa resulted in large deformation (>20%). In view of these results from the initial experiments, bonding was carried out at 900°C for 1 h under pressure of 10 MPa. The quality of the bond was checked in each case using optical microscope and EPMA. The metallographic and microanalytical examinations of the specimens indicated that the width of the diffusion zone prior to diffusion annealing was negligible as compared to that obtained after diffusion annealing. The diffusion couples thus prepared were sealed in quartz capsule under helium atmosphere and subsequently diffusion annealed in a preheated furnace controlling the temperature within ±1°C in the temperature range 750–940°C and for periods between 1 and 240 h.

Table 1
Chemical composition of the materials used

403 steel (wt%)				
Cr	Mn	C	Si	Fe
12.0	1.0	0.15	0.5	Balance
Zr–2.5Nb				
Nb (wt%)	Oxygen (ppm)	Fe (ppm)	Hydrogen (ppm)	Nitrogen (ppm)
2.51	1092	1250	<10	30

2.2. Metallography

The annealed diffusion couples were mounted and polished perpendicular to the diffusion zone. The zirconium end of the diffusion couple was etched in a solution containing 40% HNO_3 + 3% HF + 57% H_2O and stainless steel end was electrochemically etched in oxalic acid solution. The couples were examined under the optical microscope.

2.3. Electron microprobe analysis

The marked regions of the polished and unetched diffusion couples of Zr–2.5Nb/403 steel annealed at different temperatures were analysed with the EPMA (Camebax-Micro) operating at beam energy of 15 KeV with a stabilised beam current of 100 nA. The specimens were loaded in the microprobe such that the diffusion interface was perpendicular to X-axis of the specimen stage and hence parallel to the electron beam. Both point counting and automatic line scans were employed to record the concentrations of Zr, Nb, Fe and Cr. Lithium fluoride (LiF) crystal was used for dispersion of Fe(Kα), Cr(Kα), and pentaerythritol (PET) crystal was used for dispersing Zr(Lα), and Nb(Lα) lines. The raw intensity data thus obtained were corrected for atomic number (Z), absorption (A) and fluorescence (F) effects to get true concentration profiles using standard ZAF correction software.

2.4. Transmission electron microscopy

TEM was employed to investigate the microstructural details of Zr–2.5Nb/403 steel diffusion interface. Several sections were taken close to the interface region of both Zr–2.5Nb and 403 steel. Discs of 3 mm diameter were punched out from thin specimens. The specimens were thinned by jet Electro thinning at 20 V in a solution containing 6 ml perchloric acid + 34 ml *n*-butyl alcohol + 60 ml methanol, maintained at the temperature of −35°C.

3. Results and discussions

3.1. Microstructure of the parent materials

3.1.1. 403 Stainless steels

The material employed in the present investigation was received as 10 mm thick sheets, which had a prior heat treatment of oil quenching at 950°C and then tempering at 630°C for 6 h. The microstructure of the as-received material is shown in Fig. 1. The microstructure clearly indicates that the quenching treatment produces a martensitic structure. In addition, the microstructure clearly shows the presence of prior austenite grain structure. TEM studies on these specimens confirm that the martensite produced is of the lath type and also contains high density of dislocations within them. In addition, a fine distribution of carbides primarily of lenticular shape located at prior austenite grain boundaries, packet boundaries and also at lath boundaries, is observed.

3.1.2. Zr–2.5 wt% Nb

The pressure tube material Zr–2.5Nb that was received from NFC Hyderabad was β-quenched at 1000°C and then hot extruded at 800°C. This material was further pilgered in two stages, vacuum annealed at 550°C for three days and finally autoclaved at 400°C for 72 h. The details of the thermo-mechanical treatments are discussed elsewhere [10]. The alloy consists of fine two-phase structure of α and β plates. It was difficult to resolve the fine structure by optical microscopy. The bright field image (BFI) from the TEM is shown in Fig. 2. The bright and dark phase regions represent α and β regions, respectively. The β phase is located at α/α grain boundaries and this feature is evident from the micrograph.

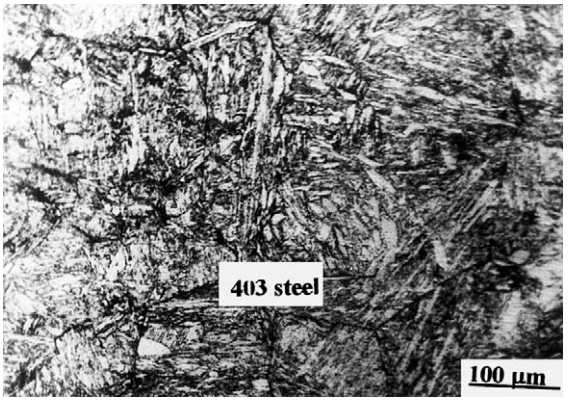

Fig. 1. Optical micrograph of the 403 steel in the as-received condition. The microstructure shows a lath type martensite structure and also prior austenite grain structure.

Fig. 2. Bright field image of the Zr–2.5Nb in the as-received condition. The micrograph clearly shows the β phase at the α/α grain boundaries.

3.2. Characterisation of the reaction zone of the as-bonded specimen

A typical optical micrograph of the bonded specimen at 900°C for 1 h, in the unetched condition is shown in Fig. 3. The micrograph clearly indicates the absence of any discontinuities, micro-pores, intermetallic compounds and suggests that a potentially sound bond is achieved at this bonding temperature. The composition penetration profiles for Zr, Nb, Fe and Cr across the diffusion couple as established by EPMA are shown in Fig. 4. These profiles indicate negligible interdiffusion at the interface. The smooth profiles of Zr, Nb, Fe and Cr,

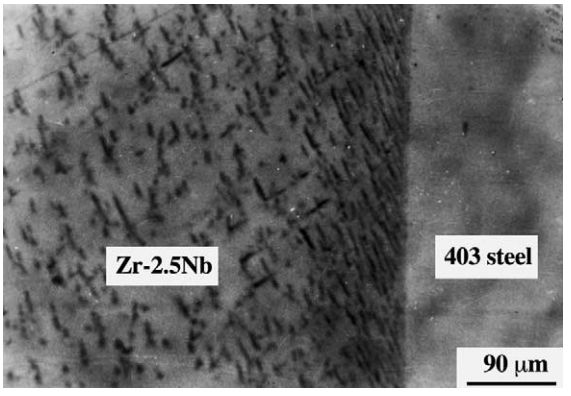

Fig. 3. Optical micrograph of the as-bonded specimen at 900°C for 1 h in the unetched condition.

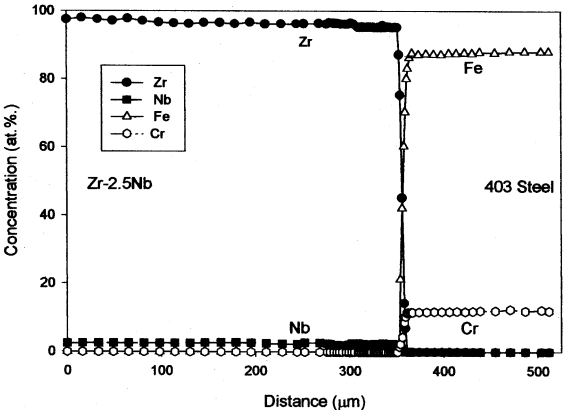

Fig. 4. Concentration profiles of various elements across the diffusion zone for as-bonded specimen at 900°C for 1 h.

and the absence of any steps also suggest that no intermetallic compound is formed.

3.3. Characterisation of the reaction zone for the specimens annealed in the temperature range 750–870°C

The polishing behavior of these specimens is quite complex. This has invariably resulted in the problem of focusing at the interface. In view of this difficulty, the micrograph of the interface region is taken at lower magnification while those of the parent materials are taken at higher magnification. A typical optical micrograph of the specimen annealed at 870°C for 240 h is shown in Fig. 5(a) along with the microstructures of the parent materials, Zr–2.5Nb and 403 steel, at higher magnification in Figs. 5(b) and (c), respectively. The microstructure of interface region (Fig. 5(a)) clearly shows parent material, Zr–2.5Nb, diffusion zone consisting of a bright layer and iron-based solid solution (dark region) along with the parent 403 steel. The micrograph (Fig. 5(b)) clearly indicates substantial change in the microstructure on the Zr–2.5Nb compared to the as-bonded specimen (Fig. 3). There is no such change in the microstructural features on the 403 steel side (Fig. 5(c)). However, an increase in the extent of tempering is noticeable compared to the as-bonded specimen. The Zr–2.5Nb side clearly shows a two-phase structure of α (bright phase) and β.

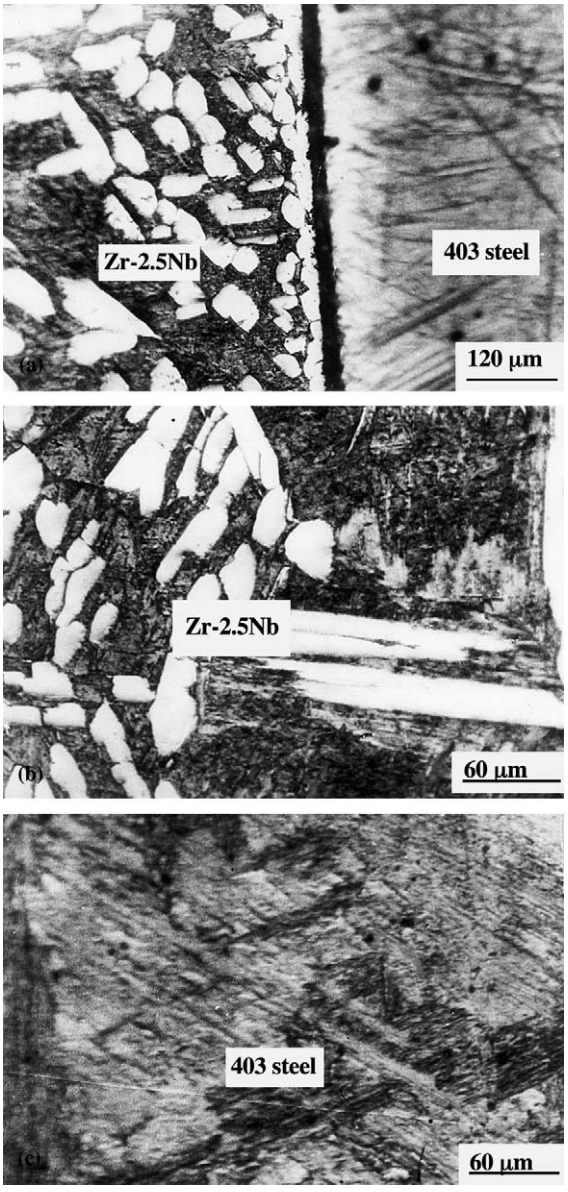

Fig. 5. Optical micrograph of the specimen annealed at 870°C for 240 h (see text for description): (a) interface region; (b) parent material Zr–2.5Nb; (c) parent 403 steel.

The bright layer in the diffusion zone has the appearance same as that of α phase in parent Zr–2.5Nb

and could be a stabilised α layer. Similar layer has been reported by Waymen et al. [9] on the Zr–2.5Nb side in the diffusion couple of 403 steel/Pt (interlayer)/Zr–2.5Nb annealed at 1100°C. It has also been reported that this stabilised α layer is richer in Pt than the bulk Zr–2.5Nb alloy. Formation of stabilised α layer in the present studies could be due to the diffusion flux of Fe, Cr from 403 steel and diffusion of oxygen from Zr–2.5Nb, which contains about 1000 ppm of oxygen.

The qualitative nature of the microstructure of the reaction zone and the parent materials corresponding to the couples annealed at 750°C, 800°C and 850°C remains nearly same as that of the diffusion couple annealed at 870°C. However, layer of α phase close to the reaction zone, which is rather discontinuous at 750°C becomes progressively continuous with increase in the temperature. The thickness of this α layer at various temperatures is listed in Table 2. It is seen from Table 2 that the thickness of the α layer increases with increase in annealing temperature.

The microstructure of Zr–2.5Nb away from the diffusion zone shows a fine distribution of α and β along with coarser α phase. The size of the coarse α phase in the matrix grows substantially with increase in the temperature of annealing. It can be seen from the Zr–Nb phase diagram (Fig. 6), that for all the couples annealed in the temperature range 750–870°C, the Zr–2.5Nb side of the diffusion couple is in $(\alpha + \beta)$ phase field. During subsequent cooling the β Zr phase transforms and results in fine plate type α phase, which can be seen in the optical micrograph. It is also seen that volume fraction of coarse α phase increases with decreases in the annealing temperature. The Zr–Nb (Fig. 6) phase diagram suggests that the volume fraction of α phase decreases with increase in temperature, confirming the experimental observation.

The concentration profiles corresponding to Cr, Fe, Zr and Nb for the diffusion couple annealed at 870°C for 240 h is shown in Fig. 7. These profiles show the formation of two distinct phases corresponding to the stabilised α layer and iron-based solid solution. The stabilised α layer is rich in Fe as compared to parent Zr–2.5Nb. The nature of the profiles for the couples annealed at lower temperatures remains similar. The widths of the solid solution region as estimated from the composition profiles for different temperatures of annealing are listed in Table 2. It can be seen that the width of the reaction zone increases with increase in the temperature of annealing. The mutual solubilites of Zr in Cr, Fe and also that of Cr and Fe in Zr estimated from these profiles are well within the solubility limits of the corresponding binary phase diagrams [11]. A closer view of the concentration penetration profiles does indicate that diffusion of iron and chromium is substantial in the Zr–2.5Nb as compared to the diffusion of Zr and Nb in the 403 steel side. No marker experiments were performed in these investigations. Most of the reaction zone is situated close to the Zr–2.5Nb side. This could be ascertained by considering the original interface as the unbonded region of the couple at the extreme top edge of it. The diffusion zone is mostly (>90%) on Zr–2.5Nb side rather than on the steel side.

Table 2
Widths of the diffusion zone and α layer in the Zr–2.5Nb/403 steel diffusion couples annealed at different temperatures for 240 h

S.No	Temperature (°C)	Width of the solid solution (μm)	Width of the α layer (μm)
1	750	16	10
2	800	18	15
3	850	22	20
4	870	22	30
5	900	100	40

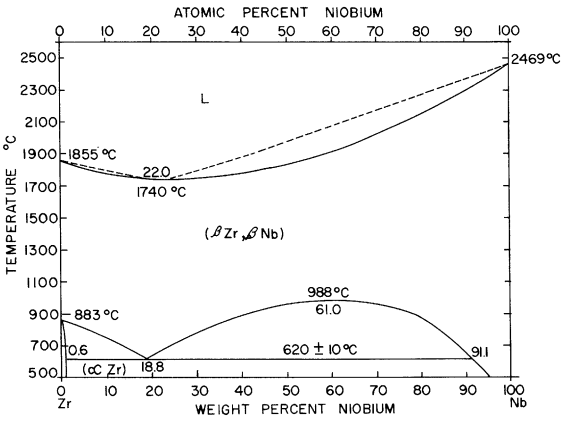

Fig. 6. Phase diagram of the Zr–Nb system [11].

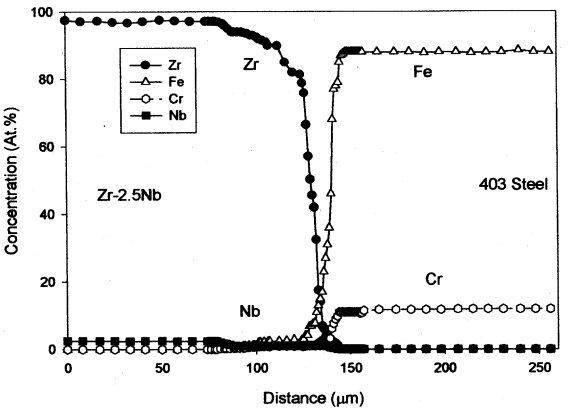

Fig. 7. Concentration profiles of various elements across the diffusion zone for the specimen annealed at 870°C. The profiles are taken from the regions devoid of α layer.

Diffusion reaction between these complex alloys should lead to the formation of several compounds. The system consists of several alloying elements viz. Zr, Nb, Fe, Cr and C. In the present analysis carbon is ignored due to relatively smaller concentration of carbon, i.e., 0.15 wt% in 403 steel. The binary systems Zr–Fe, Zr–Cr, Nb–Fe and Nb–Cr do show several intermetallics compounds [11]. However, the experimental observation does indicate the absence of binary or ternary intermetallic compounds in the diffusion zone. The absence of these compounds could be possibly due to the nucleation and subsequent growth problems [15–17]. The diffusion reaction between Zr–2.5Nb/403 steel is extremely sluggish. The reaction zone is maximum of 140 μm for the specimen bonded at 900°C for 240 h. Similar sluggish behavior is also reported in Zr/Fe system [18]. This sluggishness is possibly due to the non-attainment of equilibrium concentrations at the phase boundaries due to large incubation periods and also due to small diffusion coefficients.

3.4. Characterisation of the reaction zone for the specimens bonded at 900°C

The nature of the reaction zone for the specimen bonded at 900°C for 240 h is similar to that of the diffusion couples annealed at lower temperatures. The microstructure on Zr–2.5Nb side indicates a continuous layer of α phase of thickness (40 μm) close to the reaction zone. In addition, coarser α phase is also observed at the grain boundaries. However, there is substantial difference in the microstructures of the parent materials. The optical micrographs of the parent materials, corresponding to Zr–2.5Nb and 403 steel for the specimen bonded at 900°C for 240 h is shown in Figs. 8(a) and (b), respectively. The growth of massive α phase in Zr–2.5Nb at the grain boundaries can be seen in Fig. 8(a). The formation of a very fine martensitic structure on the 403 steel side along with large grains grain boundaries of prior austenite phase can be noticed in the Fig. 8(b). This result is consistent with the microstructure of the as-bonded specimen except that for the austenite grain size. This change in the microstructure in the 403 steel is essentially due to larger annealing time at 900°C for 240 h.

The Zr–Nb phase diagram (Fig. 6) does indicate that at 900°C, Zr–2.5Nb alloy is expected to be in complete β phase. It is also expected that this alloy produce a fine martensitic structure during quenching from 900°C to room temperature. The experimental observation is contrary to this and shows the formation of plate type α phase close to the reaction zone and also coarser α phase in the Zr–2.5Nb alloy. However, the volume fraction of this α phase is substantially reduced as compared to that of the couples annealed at 870°C (Fig. 5(a)).

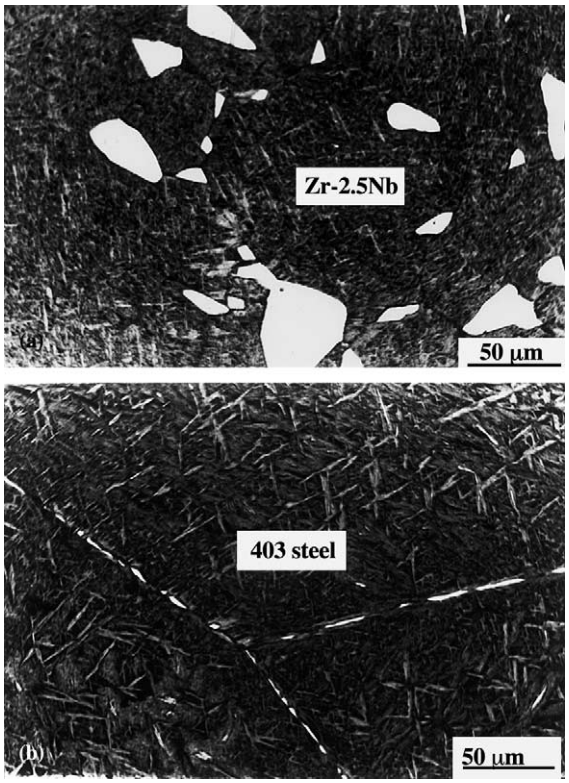

Fig. 8. Optical micrograph of the specimen annealed at 900°C for 240 h (see text for description): (a) parent material Zr–2.5Nb; (b) parent 403 steel.

A detailed TEM investigation was carried out close to the reaction zone on the Zr–2.5Nb side of the diffusion couple annealed at 900°C. A typical BFI is shown in Fig. 9. Two distinct regions separated by a straight interface boundary are seen. The region marked 'A' shows a single phase structure. The SAD patterns obtained from this region confirmed it as α phase. Internal features were not observed within this α phase. The other region marked as 'B' is showing a plate type α phase structure. The SAD patterns obtained from α/α interface regions confirm the presence of the β phase in the form of thin stringers. BFI taken at higher magnification is shown in Fig. 10. It can be seen from this micrograph that at the interface of a single phase (α) and two phase regions (α + β), β phase stringers from two phase region are growing into the single phase region. Presence of β in the form of stringers or growing of β stringers from the two phase α/β to the single phase region could be attributed to the fact that the interface energy of the α/β interface could be lower than the α/α or β/β type interface. TEM results also confirm that the coarser phase is only α phase.

These interesting results can be understood based on the Zr–O [11] and Zr–Nb (Fig. 6) phase diagrams. It can

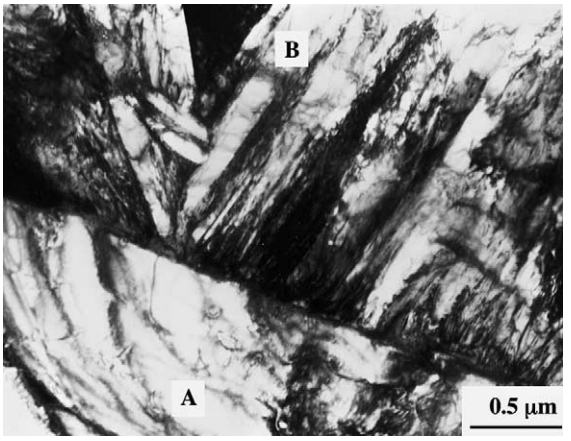

Fig. 9. Bright field micrograph taken close to the reaction zone on the Zr–2.5Nb side of the diffusion couple annealed at 900°C for 240 h. The region marked as A shows a single phase structure and the region marked B shows a plate type structure.

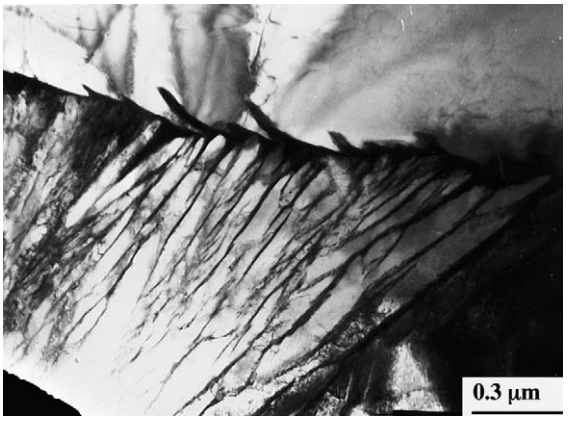

Fig. 10. Bright field micrograph corresponding to the region B taken at higher magnification. The growth of the β phase in the form of thin stringers growing at the α/α interface.

be seen from Zr–O phase diagrams that the α to β transformation is substantially modified by the presence of oxygen in zirconium. The transformation temperature for a typical concentration of 1% of oxygen in zirconium, changes from 863°C to 960°C. Bell and Evans [12] have reported that the $(\alpha+\beta)/\beta$ transformation temperature to be around 920°C for Zr–2.5Nb with oxygen concentration of about 1000 ppm. In the present investigation Zr–2.5Nb parent material contains 1092 ppm of oxygen (Table 1). The presence of this amount of oxygen could have changed the α to β transformation temperature well above 900°C. Hence at the annealing temperature of 900°C, the Zr–2.5Nb is in fact in the $\alpha+\beta$ phase field and not in complete β. The similarity in the microstructure for the couples bonded at 900°C and at 870°C is possibly due to the upward shift of the $(\alpha+\beta)/\beta$ transformation temperature caused by the presence of interstitial oxygen impurity. However, the microstructure for as-bonded specimen (900°C for 1 h) did not show the presence of any coarse α (Fig. 3). This result could be due to very short annealing time, i.e., 1 h at 900°C. The volume fraction of the α phase formed for the couple annealed at 900°C for 240 h is smaller compared to that formed at 870°C. This fact is clearly evident from the microstructures of the couples annealed at 870°C and 900°C (Figs. 5 and 8). Lower volume fraction of α phase with increase in temperature has been discussed based on the Zr–Nb phase diagram in Section 3.3.

The concentration profiles corresponding to Cr, Fe, Zr and Nb for the diffusion couple annealed at 900°C for 240 h are similar to those annealed at lower temperatures. However, the width of the diffusion zone is about 140 μm, which is substantially larger as compared to the widths of the diffusion zones obtained at lower temperatures (Table 2). The phase diagram of Fe–12%Cr steel (a composition close to 403 steel) indicates that 403 steel with 0.12%C is in α phase up to 840°C and transforms to γ phase above 880°C [13]. This large diffusion zone at 900°C may be due to large diffusivities at temperatures observed close to the transformation temperature. Similar high diffusivities have been observed for Co, Cr and W in steel in the temperature range 950°C and 1100°C [14]. This abnormal behavior is possibly due to the effect of internal interfaces that appear during the phase transformation [14].

3.5. Characterisation of the reaction zone for the specimens bonded above 900°C

The microstructures of the parent materials 403 stainless steel and Zr–2.5Nb away from the diffusion zone for the couple bonded at 940°C are similar to that of the specimens annealed at 900°C for 240 h. These results conclusively indicate that the presence of oxygen of about 1092 ppm raises the α–β transformation temperature above 940°C. However, the diffusion zone indicates a structure typical of eutectic solidification. It is a clear evidence of localised melting occurring at the interface during diffusion bonding. In order to determine the possible precise bonding temperature at which localised melting could result, specimens were annealed at 920°C, 930°C and 940°C for 15 min. The specimens annealed at 920°C and 930°C for 15 min showed no sign of melting. However, the specimen annealed at 940°C for 15 min showed localised melting suggesting that this temperature and time are adequate for localised melting to take place. The composition of the eutectic phases established by EPMA appears more close to the eutectic phases in Zr–Fe system [11]. The eutectic temperature of Zr–Fe system occurs at 928°C [11]. However the differ-

Table 3
Composition of various phases in the parent Zr–2.5Nb alloy annealed at different temperatures

S.No	Temperature (°C)	α phase				Matrix	
		Zr (wt%)		Nb (wt%)		Zr (wt%)	Nb (wt%)
		Diffusion couples	Phase diagram	Diffusion couples	Phase diagram	Diffusion couples	Diffusion couples
1	750	98.7	99.2	1.30	0.8	93.60	6.40
2	800	99.01	99.4	0.99	0.6	94.97	5.03
3	850	99.05	99.5	0.95	0.5	95.20	4.80
4	870	99.10	100.0	0.90	0.0	95.80	4.20
5	900	99.95	100.0	0.05	0.0	96.10	3.90

Point count analysis by EPMA are taken from the α phase and matrix in Zr–2.5Nb.

ence observed in the present investigation is possibly due to the presence of several alloying elements or overheating required for melting to take place.

3.6. Composition of the α and β phases in the Zr–2.5Nb alloy

The composition of the α and β phases as reported in the Zr–Nb phase diagram (Fig. 6) and those estimated from the diffusion couples by spot analysis are listed in Table 3, along with the compositions of Zr and Nb in the matrix. It should be mentioned that a fine distribution of α and β phases in the matrix (dimensions less than 1 μm) could not be resolved by EPMA and these values are to be considered as a net average composition of the α and β phases with the specific volume fractions.

It can be seen from Table 3, that the composition of Zr in the α phase estimated from the point count analysis increases with increase in the temperature from 750°C to 900°C and correspondingly there is decrease in the composition of Nb. These results are consistent with the Zr–Nb phases diagram (Fig. 6) except that the compositions do not always reach the equilibrium values. It is likely that prevailing non-equilibrium effects cause the variation in the composition of the phases and deviate substantially from those of equilibrium phase diagram values [15].

3.7. Layer growth kinetics

The width of a phase X, grown in diffusion zone follows the relation

$$X = kt^{1/n}, \tag{1}$$

where k is reaction constant, t is time in seconds and 'n' is reaction index. For the diffusion controlled reactions n has the value of 2. The temperature dependence of the reaction constant follows Arrhenius relationship and temperature dependence of phase width can be expressed as

$$X = k_o t^{1/2} \exp(-Q_p/RT), \tag{2}$$

where Q_p is the activation energy for the phase growth and T is the temperature of the diffusion anneal.

The widths of the solid solution region and those of stabilised α layer are plotted against reciprocal of the temperature of the diffusion anneal in Fig. 11. The values of the diffusion widths at 900°C are excluded for this purpose as the growth at this temperature shows

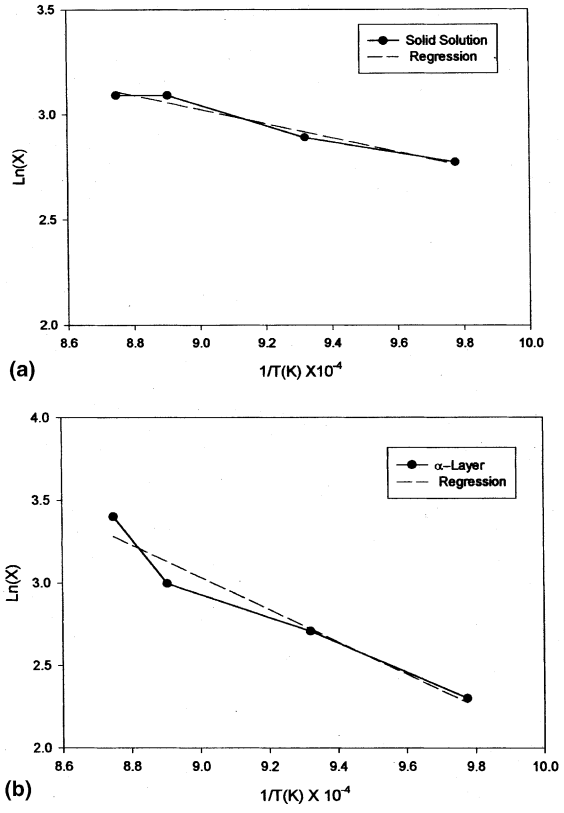

Fig. 11. Temperature dependence of diffusion widths of phases in Zr–2.5Nb/403 steel system: (a) solid solution phase; (b) stabilised α layer.

abnormal behavior as explained in Section 3.4. The plots are linear as expected. The values of the activation for the phase growth and k_o have been have been estimated from the slope and intercepts of these plots respectively using least-mean squares analysis.

The values of k_o for solid solution is 4.6×10^{-7} m/s^2 and that of the stabilised α layer is 1.5×10^{-4} m/s^2. The activation energy of phase growth for solid solution (28.14 kJ/mol) is smaller than that for stabilised α layer (81.94 kJ/mol) indicating the faster growth of solid solution. The activation for phase growth can be compared with the activation energy of diffusion. For diffusion controlled reaction, diffusion distances (X) can be related to diffusion parameters as

$$X^2 = D_0 \exp(-Q/RT), \tag{3}$$

where D_0 is frequency factor and Q is activation energy for diffusion.

Comparing Eqs. (2) and (3) we have

$$Q = 2Q_p. \tag{4}$$

In the present case activation energy for growth of stabilised α layer is 81.9 kJ/mol and accordingly activation energy for diffusion in α phase should be 163.9 kJ/mol. This value of activation energy for diffusion is comparable to the value of activation energy for diffusion of Fe in α-Zr (196.8 kJ/mol) [19]. This shows that the growth of the α phase is controlled by diffusion of Fe in Zr, which is a major constituent of steel. Similarly the activation energy for diffusion in solid solution should be 56.3 kJ/mol. The value of activation for diffusion in solid solution is very low. This may be due to nearly constant and low values of diffusion widths.

4. Conclusions

1. Diffusion bonding of 403 steel to Zr–2.5wt% Nb could be carried out at a pressure of 10 MPa, at 900°C for 1 h.
2. The microstructure of the bonded region on 403 steel side is essentially a martensitic structure and remains nearly unaltered during annealing. However, the microstructure of the Zr–2.5Nb changed substantially, leading to the formation of coarser α phase.
3. The concentration profiles of the main diffusing elements Zr, Nb, Fe, and Cr are well within the solid solubility limits and could be understood based on the respective binary phase diagrams. The concentration profiles were smooth showing no signs of the formation of any intermetallic compounds in the diffusion zone. The binary phase diagram of Zr–Fe, Zr–Cr, Nb–Fe, and Nb–Cr do show several intermetallic compounds. The absence of these phases could be attributed to the non-attainment of the required stoichiometry due to the nucleation and growth problems.
4. Diffusion reaction is very sluggish and this sluggishness is attributed to non-attainment of equilibrium concentrations at the phase boundaries due to large incubation periods.
5. Local melting occurred for the specimens annealed at the temperature of 940°C for 15 min. This is essentially due to the eutectic reaction between zirconium and iron.
6. Layer growth kinetics of stabilised α phase and the solid solution have been established. The activation energy for phase growth for solid solution (28.1 kJ/mol) is smaller than that for stabilised α layer (81.9 kJ/mol). The activation energy for diffusion in α phase is comparable to that of diffusion of Fe in Zr. This shows that the growth of the α phase is governed by the diffusion of Fe in Zr which is major component of the steel.

Acknowledgements

The authors are grateful to Dr S. Banerjee, Director, Materials Group and Dr P. Mukhopadhyaya, Head, Physical Metallurgy Section for their keen interest in this work. The authors also thank Mr Amit Chaubey, graduate student, College of Engineering, University of Pune, Pune, for his help in carrying out some of the experiments.

References

[1] P.Gr. Lucuta, I. Patru, F. Vasiliu, J. Nucl. Mater. 99 (1981) 154.
[2] S. Honda, Nucl. Eng. Des. 81 (1984) 159.
[3] H.I. Shaaban, F.H. Hammad, J.L. Baron, J. Nucl. Mater. 71 (1978) 277.
[4] G.B. Kale, K. Bhanumurthy, K.C. Ratnakala, S.K. Khera, J. Nucl. Mater. 78 (1986) 73.
[5] K. Bhanumurthy, J. Krishnan, G.B. Kale, S. Banerjee, J. Nucl. Mater. 217 (1994) 67.
[6] K. Bhanumurthy, J. Krishnan, G.B. Kale, R.K. Fotedar, A.R. Biswas, R.N. Arya, J. Mater. Proc. Tech. 54 (1995) 322.
[7] K. Bhanumurthy, G.B. Kale, J. Krishnan, BARC Internal Report, BARC/1997/I/002.
[8] M.H. Cooper, CAN Conference, Ottawa, June 1983, 63.
[9] M.L. Wayman, R.R. Smith, M.G. Wright, Metall. Trans. A 17 (1986) 429.
[10] D. Srivastava, G.K. Dey, S. Banerjee, BARC Internal Report, BARC/1992/011.
[11] T.B. Massalski, Binary Alloy Phase Diagrams, 2nd Ed., American Society for Metals, Metals Park, OH, 1990.
[12] L.G. Bell, W. Evans, AECL Report, AECL/1961/1395.
[13] E.E. Thum, Book of Stainless Steel, 2nd Ed., American Society for Metals, Metals Park, OH, 1935.
[14] P.L. Gruzin, Probl. Metalloved. Fiz. Metall. 4 (1955) 275.

[15] K. Bhanumurthy, G.B. Kale, S.K. Khera, M.K. Asundi, Metall.Trans. A 21 (1990) 2897.
[16] G.B. Kale, R.V. Patil, P.S. Gawde, J. Nucl. Mater. 257 (1998) 44.
[17] J. Philibert, Def. Diffusion Data 143–147 (1997) 529.
[18] K. Bhanumurthy, G.B. Kale, S.K. Khera, J. Nucl. Mater. 185 (1991) 208.
[19] E.A. Brandes, G.B. Brook (Eds.), Smithels Metals Reference Book, Butterworths, London, 1992.